Photoreflectance and piezophotoreflectance studies of strained-layer $In_xGa_{1-x}As$-GaAs quantum wells

G. Arnaud, J. Allègre, P. Lefebvre, and H. Mathieu
Groupe d'Etudes des Semiconducteurs, Université des Sciences et Techniques du Languedoc, Case Postale 074, Montpellier CEDEX 05, France

L. K. Howard
Strained-Layer Structures Research Group, University of Surrey, Guilford, Surrey GU2 5XH, England

D. J. Dunstan
Physics Department, University of Surrey, Guildford, Surrey GU2 5XH, England
(Received 12 July 1991; revised manuscript received 25 June 1992)

In this paper we present an investigation of the optical transitions in strained $In_xGa_{1-x}As$-GaAs single and multiple quantum wells, for indium content $x \simeq 10\%$ and 20% and various well widths. The uniaxial stress dependence of reflectance and photoreflectance spectra permits unambiguous assignment of the experimental features to electron-heavy-hole and electron-light-hole excitonic transitions. Calculated transition energies are compared with the measured values. In these calculations, in the envelope-function formalism, the misfit-strain-induced coupling between the Γ_8 light-hole and the Γ_7 split-off valence bands is taken into account and the valence-band offset ratio is chosen as an adjustable parameter. By fitting all the experimental results to our calculations, the heavy-hole valence-band offset fraction Q_{vh} is determined to be about 0.34. This implies that these quantum wells are type I for the electron-heavy-hole system and type II for the electron-light-hole system, with the electrons and the heavy holes confined in the $In_xGa_{1-x}As$ layers and the light holes in the GaAs barrier regions.

I. INTRODUCTION

In recent years there has been considerable interest in the strained-layer $In_xGa_{1-x}As$-GaAs system from both fundamental and applied points of view. The optical properties of the InGaAs-GaAs system have been studied in single quantum wells (SQW's),[1-5] multiple quantum wells (MQW's),[6-16] and superlattices.[17] Early reports[6] established the possibility that the system is mixed type I_h/II_l due to strain. That is, the electrons and heavy holes are confined in the $In_xGa_{1-x}As$ layers forming a type-I heterostructure, and because of the strain, the light holes may be confined in the GaAs layers forming a type-II system. Such a type-II configuration for the light holes has been clearly demonstrated by Gerard and Marzin[18] using isoelectronic substitution in each layer. Several other experiments[1,2,7-11] are in agreement with these reports; however, the studies by Menendez *et al.*,[5] using a light-scattering method and photoluminescence excitation spectroscopy, contradict these experimental results, presenting a pure type-I band alignment where both light and heavy holes are confined in the $In_xGa_{1-x}As$ layer. This disagreement corresponds to an uncertainty in the band offset. Band offset ratios Q_v/Q_c are reported over the range 0.6/0.4 to 0.15/0.85. These values are given under two different definitions, depending on whether the reference band-gap difference (ΔE_g) corresponds to the strained materials or to the unstrained materials. Band offset ratios determined from x-ray photoemission spectroscopy (XPS) experiments[19] are 0.15/0.85 and theoretical predictions[20-22] range from 0.11/0.89 to 0.28/0.72. High-pressure photoluminescence studies[23] of $In_xGa_{1-x}As$-$Al_xGa_{1-x}As$ structures gave 0.40/0.60 for the (strained $In_xGa_{1-x}As$)/(unstrained GaAs) band offset ratio.

The aim of the present work is thus to obtain reliable information about the band lineup in this system from a quantitative analysis of the low-temperature reflectance and photoreflectance spectra of several $In_xGa_{1-x}As$-GaAs QW's with different well sizes and indium contents. All of the features observed in the experimental spectra are clearly identified via their uniaxial stress induced energy shift, which allows us to select between heavy-hole, and light-hole excitons. Moreover, the transition energies can be computed using the envelope-function formalism and taking account of the misfit-strain-induced coupling between the Γ_8 light-hole and the Γ_7 split-off valence bands. Such calculations show that the energy of light-hole excitons is very sensitive to the value of the band offset ratio Q_{vh}. Then, by fitting the calculated transition energies to the experimental ones, we extract a reliable value of 0.34 for Q_{vh} defined as $Q_{vh} = \Delta E_{vh}/\Delta E_{gh}$, where ΔE_{vh} is the quantum-well depth for the heavy holes and ΔE_{gh} the band-gap difference between the strained $In_xGa_{1-x}As$ well and the GaAs barrier.

In the following, the theoretical background of our study is presented. Next, the experiments are described, analyzed, and interpreted. Conclusions appear in the final section.

 ©1992 The American Physical Society

II. THEORETICAL BACKGROUND

To calculate the energies of the electron and hole sublevels in each QW studied here, we have used a standard quantum-mechanical approach, using the envelope-function formalism. Since we intend to extract valuable information from direct comparison between measured and calculated transition energies and their stress behavior, we must correctly deal with three contributions: (i) internal and external strain effects, (ii) binding energies of the observed excitons, and (iii) sensitivity of the calculated energies upon the numerical ingredients.

A. Strain effects

When grown on a GaAs buffer, the $In_xGa_{1-x}As$ alloy sustains a biaxial in-plane compression. Since the GaAs buffer layer and substrate is very much thicker than the ternary-alloy layer and so can be taken to be unstrained, the latter experiences a tetragonal distortion resulting in a very simple form of the strain tensor:

$$e_{xx}^0=e_{yy}^0=\frac{a_1-a_2}{a_2}\ , \tag{1a}$$

$$e_{zz}^0=-\frac{a_1-a_2}{a_2}(2C_{12}/C_{11})\ , \tag{1b}$$

where a_1 and a_2 are the lattice constants of the unstrained $In_xGa_{1-x}As$ and GaAs, respectively, and C_{ij} are the elastic stiffness constants of the ternary alloy.

In case of application of an external (110) uniaxial stress, i.e., perpendicular to the natural quantization axis of the structures, the layers experience additional deformations, so that the components of the strain tensor are

$$e_{xx}=e_{yy}=\tfrac{1}{2}(S_{11}+S_{12})\sigma\ , \tag{2a}$$

$$e_{zz}=S_{12}\sigma\ , \tag{2b}$$

$$e_{xy}=\tfrac{1}{4}S_{44}\sigma\ , \tag{2c}$$

$$e_{yz}=e_{zx}=0 \tag{2d}$$

for the GaAs layers, and

$$e_{xx}=e_{yy}=e_{xx}^0+\tfrac{1}{2}(S_{11}+S_{12})\sigma\ , \tag{3a}$$

$$e_{zz}=e_{zz}^0+S_{12}\sigma\ , \tag{3b}$$

$$e_{xy}=\tfrac{1}{4}S_{44}\sigma\ , \tag{3c}$$

$$e_{yz}=e_{zx}=0 \tag{3d}$$

for the $In_xGa_{1-x}As$ layers. e_{xx}^0 and e_{zz}^0 are the strains given by Eqs. (1a) and 1(b), σ is the uniaxial stress along (110), and S_{ij} are the elastic compliance constants of the GaAs substrate.

We remark that in systems where no internal strain is present, like GaAs-(Ga,Al)As heterostructures, the application of a (110) uniaxial stress can produce anticrossing behaviors between light- and heavy-hole states whose energies shift at different rates. In such a case, a rigorous mathematical treatment of valence-band mixings is necessary.[24–27] In the present case, the (In,Ga)As layers undergo a built-in biaxial compression whose effect is to lift the degeneracy of the valence bands. Moreover, since this compression has the same symmetry as the size quantization field of the quantum well, this strain induces no mixing between light-hole and heavy-hole states. The result is that these states are just strongly split apart by the internal strain. For this reason, the application of an additional external (110) stress, of rather small relative magnitude, will not provoke any coupling between valence states, which are already separated by quite a large energy. Thus, the (110) stress induced energy shift of valence states can also be calculated by a perturbational calculation, since, as shown below, light- and heavy-hole subbands have no chance to cross each other. In fact, a correct modeling of uniaxial strain effects should include many contributions,[24–27] but this is not the purpose of this work. Rather, we are interested in using the difference between the stress-induced energy shifts of light-hole and heavy-hole exciton lines as a reliable tool for their identification.

In the ternary alloy, the internal strain shifts the conduction-band edge. However, it shifts and splits the valence-band edge, giving rise to different strain dependences of the electron to heavy-hole and electron to light-hole energy gaps:[28]

$$E_g^{e,h}=E_{g0}+\varepsilon_h-\varepsilon\ , \tag{4a}$$

$$E_g^{e,l}=E_{g0}+\varepsilon_h+\varepsilon-\varepsilon^2/2\Delta_0\ , \tag{4b}$$

where E_{g0} and Δ_0 are, respectively, the strain-free band gap and spin-orbit splitting of the ternary alloy, given at 2 K as a function of the indium content x by[29,30]

$$E_{go}(\text{eV})=E_g(\text{GaAs})-1.5837x+0.475x^2\ , \tag{5}$$

$$\Delta_0(\text{eV})=\Delta_0(\text{GaAs})-0.09x+0.14x^2\ . \tag{6}$$

The hydrostatic-pressure dependence of the band gap ε_h and the stress-induced valence-band splitting ε are given by

$$\varepsilon_h=2a\frac{C_{11}-C_{12}}{C_{11}}e_{xx}^0\ , \tag{7a}$$

$$\varepsilon=b\frac{C_{11}+2C_{12}}{C_{11}}e_{xx}^0\ , \tag{7b}$$

where a is the hydrostatic deformation potential of the band gap and b the shear deformation potential of the valence band. It is to be noted that the light-hole valence band has a nonlinear strain dependence resulting from the strain-induced coupling between the Γ_8 light-hole band and the Γ_7 spin-orbit-split band.

In these structures e_{xx}^0 is negative, so that the heavy-hole band moves up and the light-hole band moves down, relative to the unstressed valence band. Thus the structure, which is expected to be type I for the electron-heavy-hole system, may be either type I or type II for the electron-light hole system, depending on the value of the zero-stress band offset and on the magnitude of the lattice mismatch. In other words, the electrons and heavy-holes are confined in the $In_xGa_{1-x}As$ region but the light-holes may be confined in the $In_xGa_{1-x}As$ layer (type I)

or free in the GaAs barriers (type II).

The subband energies of the QW structures are calculated by using the potential well depths:

$$\Delta E_c = Q_c[E_g(\text{GaAs}) - E_{g0} - \varepsilon_h + \varepsilon] , \quad (8a)$$

$$\Delta E_{hh} = Q_{vh}[E_g(\text{GaAs}) - E_{g0} - \varepsilon_h + \varepsilon] , \quad (8b)$$

$$\Delta E_{lh} = \theta \left[\Delta E_{hh} - 2\varepsilon + \frac{\varepsilon^2}{2\Delta_0} \right] , \quad (8c)$$

where $\theta(x)=0$ for $x \leq 0$, and $\theta(x)=x$ for $x>0$. This means that, for negative values of ΔE_{lh}, the type-II transition to the GaAs valence band edge is considered.

In the absence of external stress, the calculations are rather simple. As the electrons and heavy holes are confined in the $In_xGa_{1-x}As$ layer, using the proper effective masses, the energies of the confined states can be computed within the framework of the usual envelope-function approximation (EFA) of Bastard.[31] The quantum-mechanical problem of a finite potential well also presents solutions for free states, above the edge of the well, constituting a continuum of allowed levels. Among these levels, one can identify some resonant states, presenting a maximum transmission coefficient across the low-potential layer and which give rise to a maximum overlap integral with the corresponding confined conduction states. Optical transitions involving heavy-hole states in the continuum should then be centered around these resonant energies. The computation of the resonant energies is also made within the EFA.[31]

The case of light holes is a little more difficult to deal with because of the mixing with Γ_7-related subbands. Indeed, a correct calculation of confined light-hole states, including this effect, was only recently performed:[27] it was shown that nonvanishing matrix elements between $|\frac{3}{2},\pm\frac{1}{2}\rangle$ and $|\frac{1}{2},\pm\frac{1}{2}\rangle$ valence states appear not only in the expression for the stress Hamiltonian, but also in the Luttinger-Kohn kinetic-energy operator. The result is a reduction of the confinement energy of the lower light-hole subbands by a quantity which can be large for values of the confinement energy above $\sim\frac{2}{3}\Delta_0$. Fortunately, the samples studied in this work turn out to have a potential barrier in the $In_xGa_{1-x}As$ layer for light holes, and this avoids tedious calculations: the set of allowed energy levels is then a continuum, starting from the valence-band edge in the barrier. The transmission rate of a given state across the $In_xGa_{1-x}As$ layer increases as the energy difference between the state and the top of the barrier decreases. Non-negligible overlaps with confined conduction states can therefore be reached for energies very close to the top of shallow barriers. This is the reason why the inclusion of the Γ_7 states is crucial, since it considerably reduces the barrier height, down to ~ 5 meV. We thus choose to calculate the energy of a transition between a conduction level labeled e_n and the light-hole continuum labeled l as $E(e_n - l) = E(e_n) - E_v(\text{GaAs})$, where $E(e_n)$ is the absolute energy of the nth conduction subband, and $E_v(\text{GaAs})$ the absolute energy of the GaAs valence band.

Since light- and heavy-hole states are decoupled by the internal strain, the evolution of the heavy-hole energy levels under an externally applied uniaxial stress along the (110) direction, is given by

$$\frac{\partial E_{hh}}{\partial \sigma} = a_v(S_{11}+2S_{12}) - b(S_{11}-S_{12})/2 , \quad (9)$$

where a_v and b are the $In_xGa_{1-x}As$ deformation potentials.

Here we remark that, due to the magnitude of the internal stress ($\sim$7–15 kbar), the light-hole subbands are pushed toward a situation where the carriers are not confined, as mentioned above. Moreover, as the applied stress is always small ($\sigma < 5$ kbar), we can neglect the influence of the Γ_7 states for the determination of the stress behavior of the continuum states of light holes, which then reads

$$\frac{\partial E_{lh}}{\partial \sigma} = a_v(S_{11}+2S_{12}) + b(S_{11}-S_{12})/2 , \quad (10)$$

where a_v and b are the GaAs deformation potentials.

The physical constants used in the calculation are given in Table I for GaAs and InAs. For $In_xGa_{1-x}As$ they have been linearly interpolated between the corresponding values of the binary compounds.

The structural parameters characterizing the electron and hole energy states in the QW are the well width L_w together with the well depth. The latter is a function of both the fractional alloy composition x and the band offset ratio; we used Q_{vh} defined as $Q_{vh} = \Delta E_{vh}/\Delta E_{gh}$, where ΔE_{vh} is the heavy-hole well depth and ΔE_{gh} is the band-gap difference.

B. Excitonic effects

Fitting the calculated values of the subband-gap energies to the observed optical transition requires the bind-

TABLE I. Physical constants of GaAs and InAs.

	GaAs	InAs
Lattice constant (Å)	5.6533[a]	6.0583[a]
C_{11} (10^{+2} kbar)	11.26[b]	8.33[c]
C_{12} (10^{+2} kbar)	5.71[b]	4.53[c]
C_{44} (10^{+2} kbar)	6.00[b]	3.959[b]
a (eV)	−8.0[d]	−6.0[e]
a_c (eV)	−9.3[f]	
b (eV)	−1.75[g]	−1.8[e]
d (eV)	−4.55[h]	−3.6[i]
m_e/m_0	0.0665[a]	0.023[a]
γ_1	7.65[j]	19.67[j]
γ_2	2.41[j]	8.37[j]

[a]Reference 15.
[b]Reference 32.
[c]Reference 33.
[d]Reference 34.
[e]Reference 35.
[f]Reference 36.
[g]Reference 37.
[h]Reference 38.
[i]Reference 39.
[j]Reference 40.

ing energy E_b of the confined exciton. Many authors have presented determinations of E_b for excitons confined in quantum wells, both theoretically and experimentally. Two experimental methods are currently used: one is to observe the ground and continuum excitonic states by photoluminescence-excitation spectroscopy, the other is to infer the subband gap from the extrapolation of Landau-level transitions using magneto-optical measurements. The former approach has been used by Moore *et al.*[41] to obtain direct measurements of the heavy-hole exciton binding energy in 48, 25, and 14 Å $In_xGa_{1-x}As$-GaAs wells with $x=0.15$. The latter method has been used by Hou *et al.*[16] for examples with well widths ranging from 65 to 100 Å and indium fraction ranging from 0.07 to 0.13, and by Haines *et al.*[42] for well thicknesses between 30 and 120 Å. In all cases, a model calculation is carried out in a variational framework in the envelope-function approximation; a good agreement between the experimental and calculated results is achieved. The exciton binding energy is shown to depend on indium fraction and well width. It has a maximum value at a width of about 55 Å, and decreases to the three-dimensional (3D) value in both limits of zero and infinite width. This behavior is accounted for in terms of the spatial confinement of the exciton. In our samples, from these results, we estimate the binding energy E_b for the fundamental $e1$-$h1$ exciton to be 8, 8, 8, and 5 meV in the 50-, 70-, 110-, and 270-Å QW's respectively. Though these values are not relevant for higher-lying transitions, involving excited states, we will use them, in the following, for our comparison between theory and experiments. We did so for simplicity, since we do not consider it reasonable to take the difference between experimental and computed band-to-band transitions energies as a measurement of the binding energies of the excitons. This explains some apparently random discrepancies in the comparisons of Table III (see below).

C. Influences of x and Q_{vh}

Let us consider Figs. 1(a) and 1(b) which give, for a SQW with $L_w=110$ Å, the calculated dependences of the intersubband transition energies on Q_{vh} and x. In the former figure, $x=0.18$ and Q_{vh} ranges from 0.20 to 0.60. In the latter, Q_{vh} is fixed at 0.34, while x ranges from 0.10 to 0.20. Clearly, while all the transitions are strongly x dependent, the ei-hj transitions and particularly $e1$-$h1$ are only weakly Q_{vh} dependent. This simply results from the fact that the electron-heavy-hole system is type I. In contrast, the electron-light-hole system has a type-II configuration for small Q_{vh}, and in this region the corresponding transition energy is strongly Q_{vh} dependent. As a result, in the following, the e_n-h_m transitions are used to perform optical checks of the well indium content x and well width L_w (because the nominal values are only anticipations). Then Q_{vh} is varied in order to fit the e-l transitions.

III. EXPERIMENTS

A. Samples and experimental conditions

The samples used in this study were grown by molecular-beam epitaxy (MBE) on (001)-oriented undoped GaAs substrates in a Vacuum Generators V80H MBE system. The gallium and indium beam fluxes were set using reflection high-energy electron diffraction

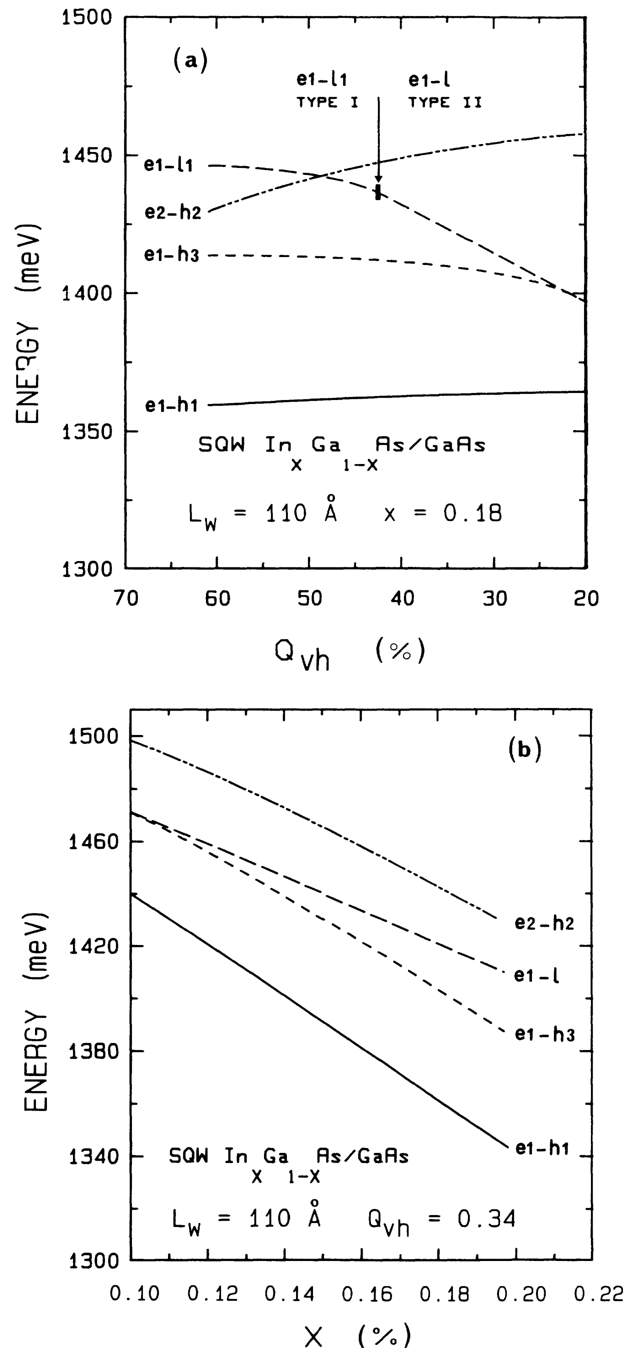

FIG. 1. Calculated values of the energies of ei-hj and $e1$-l for an $In_xGa_{1-x}As$-GaAs single quantum well as a function of the (a) valence-band offset parameter Q_{vh} and (b) indium content x.

(RHEED) oscillations, obtained from growth of GaAs on GaAs and InAs on InAs, respectively. The $In_xGa_{1-x}As$ growth rate of 1 (ML) per s was obtained by setting the GaAs and InAs growth rates to 0.9 and 0.1 $ML\,s^{-1}$, respectively for $In_{0.1}Ga_{0.9}As$, and to 0.8 and 0.2 $ML\,s^{-1}$ for $In_{0.2}Ga_{0.8}As$. Growth was carried out under an overpressure of the arsenic tetramer, As_4, which gave a beam equivalent pressure of 1.2×10^{-7} Torr, as measured by a flux monitoring ion gauge (corresponding to a flux of approximately 6×10^5 atoms $cm^{-2}\,s^{-1}$) and a group-V to group-III ratio of 5:1.

At this arsenic flux the transition temperature T_t of the GaAs surface between its As-rich $c(4\times4)$ and As-stable (2×4) RHEED reconstructions was found to be approximately 530 °C. This transition temperature is measured both after *in situ* desorption of the surface oxide and again after growth of a 700-nm GaAs buffer at T_t+49 °C. The $In_xGa_{1-x}As$ quantum wells were grown at a temperature of T_t-11 °C, since this has previously been found to be below the temperature at which significant desorption occurs[43] and gives high-optical-quality quantum wells from photoluminescence. The GaAs barrier thicknesses were insufficient to allow an increase in growth temperature and were therefore also grown at T_t-11 °C.

Sample *A* consists of one $In_xGa_{1-x}As$-GaAs single quantum well (SQW) with a nominal composition $x=0.2$ and well width $L_w=110$ Å. Sample *B* is composed of three SQW's with a nominal $x=0.1$ and $L_w=10$, 50, and 270 Å, separated by 500-Å-wide GaAs barriers. Sample *C* is a multiple quantum well (MQW) composed by three QW's with a nominal $x=0.2$, well width $L_w=70$ Å, and barrier thickness $L_B=100$ Å. All three samples were characterized by photoluminescence: the PL of sample *B* is discussed in detail in Ref. 44. In Table II are indicated the composition values for each well, corresponding to the best fit between theory and experiments. These values may differ from one layer to another within a same sample. The reason for this is that each well width is different, so that effects such as flux transients[45] when the shutter is opened, and indium segregation, are different for each well. On the other hand, it is not the case for superlattices and periodic MQW's, for which the growth conditions for each well are expected to be the same to much better than 1%.

Two critical thicknesses, t_{c1} and t_{c2}, have been identified in the $In_xGa_{1-x}As$-GaAs system.[46] A low dislocation density occurs above the smaller, t_{c1}, which is about 80 Å for $x=0.2$ and is expected to be 160 Å for $x=0.1$. However, significant plastic relaxation occurs only above the second critical thickness, t_{c2}, which is 600 Å for $x=0.2$ and theoretically predicted to be 1200 Å for $x=0.1$.[47] All of our quantum wells are below t_{c2} and so are expected to have the grown-in strain (1.4% for $x=0.2$ and 0.7% for $x=0.1$). However, all the structures are above t_{c1} and so are expected to have nonzero dislocation densities, particularly in the first $GaAs/In_xGa_{1-x}As$ interface. The accuracy with which the transitions can be fitted theoretically, without assuming any plastic relaxation, confirms that the first critical thickness is unimportant for the electronic band structure.

Reflectivity spectra were taken at 2 K in a pumped liquid-helium bath. Focused broad-band light from a tungsten lamp was reflected from the sample, imaged onto the monochromator input slit, dispersed and detected. Photoreflectivity (PR) spectra were also recorded to facilitate the observation of weak structures in the reflectivity spectra. A chopped He-Ne laser was used as the secondary source. Finally, uniaxial stress was applied in both reflectivity and PR in order to assist in the assignment of the spectral features.

TABLE II. Pertinent parameters used in the calculation. For each sample the nominal value of the well width is repeated. Q_V is the strain-free ratio of the valence- to-conduction-band discontinuity, defined in the text. The compositions and well widths have been determined by the fit to experiments. We allowed different wells in the same sample to take different compositions, as, although they might be expected to have the same values, this is far from certain.

Sample	*A* (110 Å)	*B* (270 Å)	*B* (50 Å)	*C* (70 Å)
$In_xGa_{1-x}As$ layer				
Indium content (%)	17.5	10	9	18
Layer thickness (ML)	36	95	17	24
(Å)	104	272	49	68
Biaxial in plane compression (kbar)	13	7.5	6.5	13.3
Electron well depth V_e (meV)	120	72	63	120
Heavy-hole well depth V_h (meV)	68.5	33	29	74
Light-hole barrier V_l (meV)	11	7.7	6.2	8
Ratio of the valence-to-conduction-band discontinuity				
Q_{vh} (%)	36.3	31.5	31.5	38
Q_v (%)	13	10	11	14

B. Experimental data

Shown in Figs. 2, 3, and 4 are the experimental reflectance spectra for samples *A*, *B*, and *C*, respectively. In the bulk case, it is well established that many physical quantities, such as the refractive index, effective mass and damping parameter together with additional boundary conditions, contribute in a sensitive manner to the general shape of a reflectance structure.[48] The breaking of the (001) translational symmetry in the case of QW's leads to additional complications. A quantitative fit to these spectra in terms of the exciton-polariton formalism is outside the scope of the present paper; instead, we work with the peak energies of the features. Identifiable features on the spectra in Figs. 2, 3, and 4 are labeled from 1 to *n* before identification, and *ei-hj* or *ei-lj* after the identification discussed in the next section.

The spectrum of sample *A* consists of five features associated with the 110-Å-wide SQW. Clearly, two features, 1 and 5, are stronger than the others. Sample *B* shows a series of features labeled 1–7 associated with the 270-Å-wide $(\mathrm{SQW})_\beta$ and a strong feature labeled $(1)_\beta$ associated to the 50-Å-wide $(\mathrm{SQW})_\beta$. No features were detected that could be associated with the 10-Å well. Figure 4, which corresponds to the 70-Å MQW, exhibits five features, of which three are strong. The inset shows a high-energy feature which corresponds to the direct band gap of unstrained GaAs and originates from the GaAs buffer-substrate region of the sample. This structure, which appears in the spectra of all three samples, is used as a strain gauge in the uniaxial stress experiments (see below).

Modulated spectroscopy is a powerful investigation tool for heterostructures,[49] because the high resolution of these techniques gives an accurate measurement of the optical structure. So, in addition to the reflectance measurements, we have performed photoreflectance measurements on samples *B* and *C*. Reflectance modulation is caused by the modulation of the built-in electric field in the surface potential barrier due to the photoexcited carriers. In the low-field regime the $\Delta R/R$ spectra are expressed by a derivative line shape of the dielectric function and the transition energy is simply obtained from the $\Delta R/R$ spectrum by using the well-known "three-point method" given by Aspnes.[50] If the line shape of $\Delta R/R$ is symmetric, the transition energy is located at the midpoint, otherwise the transition energy is located nearer the dominant extremum. In quantum wells, Shanabrook, Glemboki, and Beard[51] have shown that photoreflectance yields the first derivative of a Gaussian or Lorenzian line-shape function. This is related to the large exciton binding energies. However, for coupled wells in which tunneling can occur the situation is different, since carriers can be accelerated by the modulated electric field. This leads to the Aspnes third-derivative functional form[52] for the line shape. Here, however, the line shape

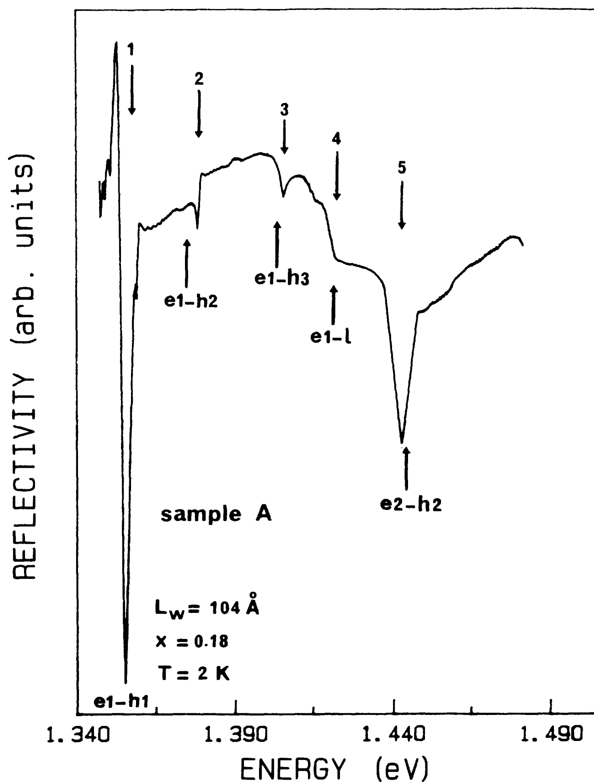

FIG. 2. Reflectivity spectrum of sample *A*. The upper arrows show the labels of the features discussed in the text. The lower arrows give the assignments of the features and show the calculated energies.

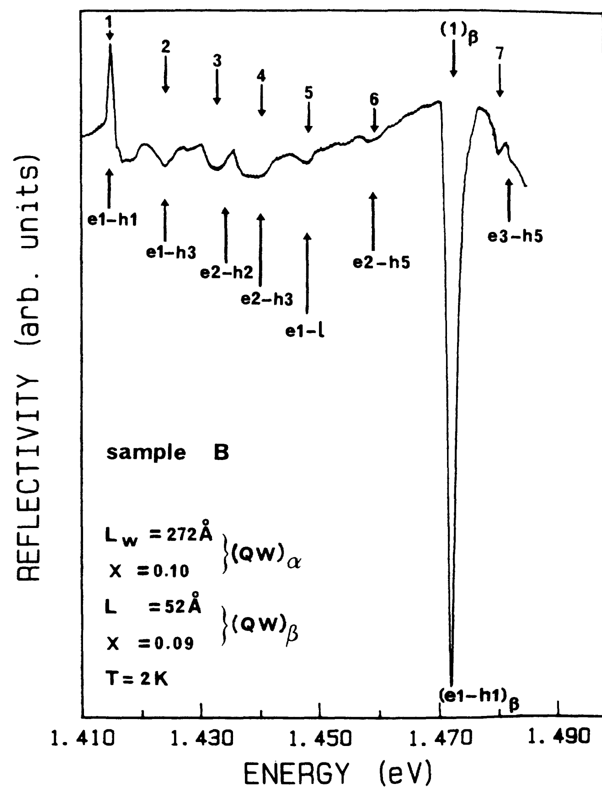

FIG. 3. Same as Fig. 2 for sample *B*. The features labeled 1–7 correspond to the 272-Å $(\mathrm{QW})_\alpha$. The feature labeled $(1)_\beta$ corresponds to the 52-Å $(\mathrm{QW})_\beta$.

is not our purpose.

A typical spectrum, given for sample C, is shown in Fig. 5. Note that this spectrum has a clear strong feature which corresponds to that labeled 1 in the associated reflectivity spectrum (Fig. 4), but also shows fine structure (labeled $1a$-$1b$) which will be discussed later. All of the features are labeled as in the reflectivity spectrum; note that feature 4 is very weak and the feature labeled y in the reflectance spectra does not appear in the photoreflectance spectrum.

In order to help the identification of the various observed features, we have performed reflectance and photoreflectance measurements under uniaxial stress. The external stress is applied in the (110) direction, so that the strain field and the (001)-oriented well potential are in crossed configuration. The magnitude of the uniaxial stress could be measured from the mechanical deformation experienced by a quartz device located under the sample and also deduced by studying the stress splitting of the three-dimensional exciton of the GaAs substrate shown in the inset of Fig. 4. The magnitudes obtained with these mechanical and electronic gauges were found to be in close agreement.

As an illustration, Fig. 6 displays the stress patterns obtained for the 110-Å SQW of sample A. The feature labeled 2, which is very weak in the zero-stress spectrum, disappears in spectra taken under uniaxial stress. Figures 7, 8, and 9 show the uniaxial stress dependences of the reflectance and photoreflectance spectra obtained from the different samples. The solid lines correspond to numerical calculations which will be discussed at length in the next section. When the stress is increased, the feature labeled 4 in samples A and C and 5 in sample B shift faster than the others. Even before the quantitative analysis of the next section, such a qualitative behavior reveals the origin of the different features. It is very well established[24–26] that, under in-plane uniaxial stress, i.e., when the strain field and the well potential are in crossed configuration, the electron-light-hole transition energies shift to higher energy faster than the electron-heavy-hole energies. As a result, we can unambiguously identify the feature labeled 4 (samples A and C) or 5 (sample B) as resulting from an electron-light-hole transition. The other features correspond to electron-heavy-hole transitions, among which the lowest energy, labeled 1, can be definitely assigned to the $e1$-$h1$ transition observed in photoluminescence.

C. Data analysis

All the pertinent parameters are gathered in Table II. The calculated and experimental transition energies are given in Table III. In order to compare the calculated and experimental values of the transition energies, the former are given as E (E_b), where E is the value of the excitonic transitions (which is to be compared to the experimental value), obtained by subtracting E_b from the inter-

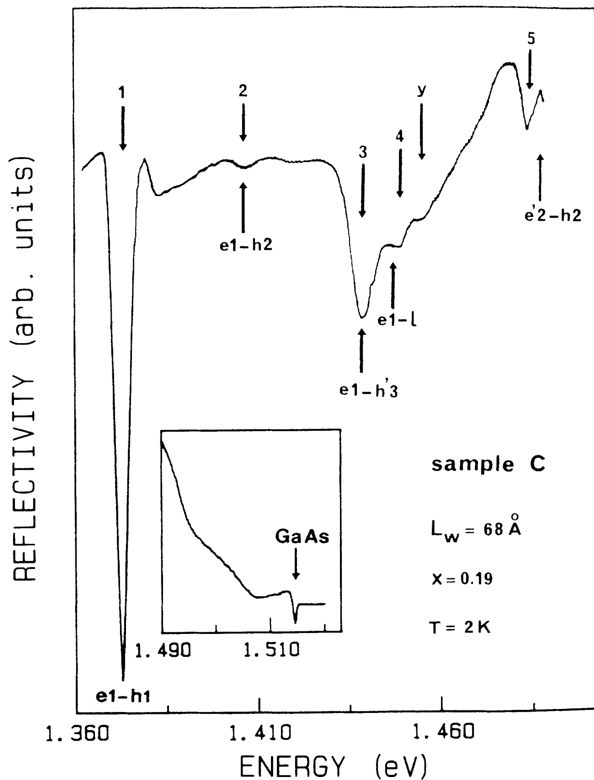

FIG. 4. Same as Fig. 2 for sample C. The prime is added to note that the level is resonant state. The inset shows a high-energy feature which corresponds to the direct band gap of unstrained GaAs.

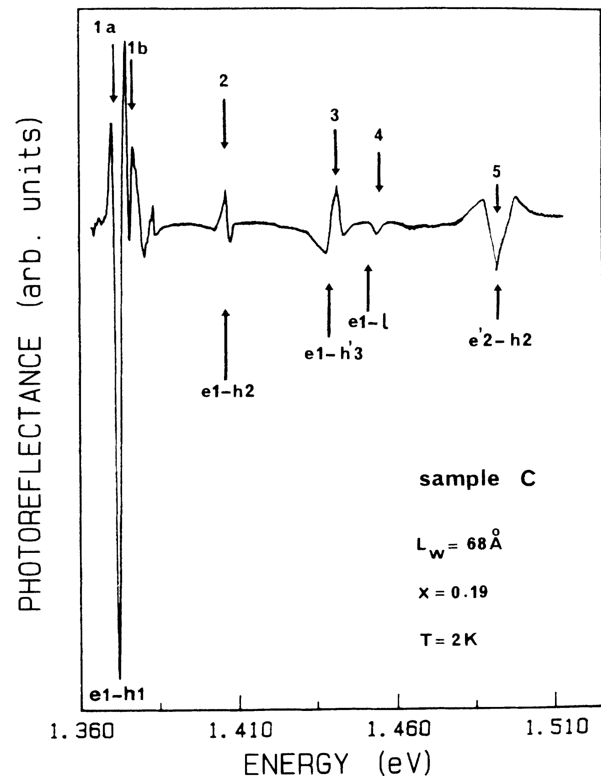

FIG. 5. Photoreflectivity spectrum of sample C.

TABLE III. Experimental and calculated values of the transition energies (in meV). The calculated values are labeled E (E_b), where E corresponds to the excitonic transition and E_b is the exciton binding energy used in the calculation. Transitions labeled $e'i$-hj (ei-$h'j$) correspond to transitions between $e'i$ ($h'j$) resonant states and hj (ei) bound states. The asterisk indicates a value masked by the strong $e1$-$h1$ feature of the 50-Å QW.

Sample	A (100 Å)		B (270 Å)		B (50 Å)		C (70 Å)	
Transition	Expt.	Calc.	Expt.	Calc.	Expt.	Calc.	Expt.	Calc.
$e1$-$h1$	1355	1355(8)	1415	1415(5)	1472	1472(8)	1372	1372(8)
$e1$-$h2$	1380	1374(8)	1419	1419(5)			1406	1407(8)
$e1$-$h3$	1406	1402(8)	1426	1424(5)				
$e1$-$h'3$							1438	1439(8)
$e2$-$h2$	1442	1443(8)	1433	1434(5)				
$e'2$-$h2$							1484	1490(8)
$e2$-$h3$			1440	1440(5)				
$e2$-$h4$			1448	1447(5)				
$e2$-$h5$			1459	1458(5)				
$e3$-$h3$			*	1465(5)				
$e3$-$h5$			1480	1481(5)				
$e1$-l	1421	1421(4)	1448	1448(4)			1448	1448(3)

subband calculated energy. For example, E $(E_b)=1355$ (8) means that $E_b=8$ meV has been taken for the exciton binding energy, and the intersubband energy difference was 1363 meV. As stated above, this should not be considered as a measurement of the effective Rydberg of the exciton, since the value of E_b has not even been varied for each transition. For this reason, better agreement would have been obtained by using smaller values for E_b, especially in the case of "forbidden" transitions, but we wanted to avoid tedious and confusing discussion on this point.

Good agreement with experiment is obtained for parameter values for which the heavy holes are confined in the $In_xGa_{1-x}As$ layer, with a potential well given by V_h in Table II, whereas the light holes are located in the GaAs by a potential barrier given by V_l in Table II, mak-

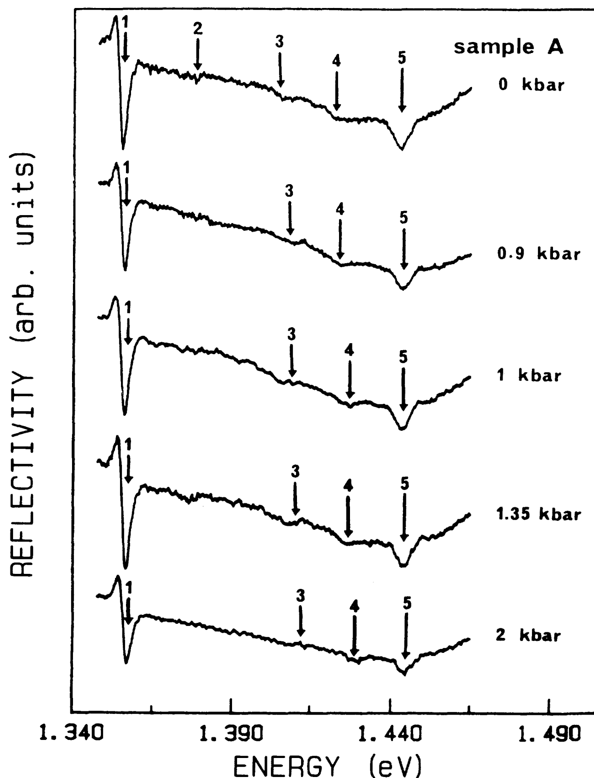

FIG. 6. Typical reflectance spectra of sample A for stress between 0 and 2 kbar.

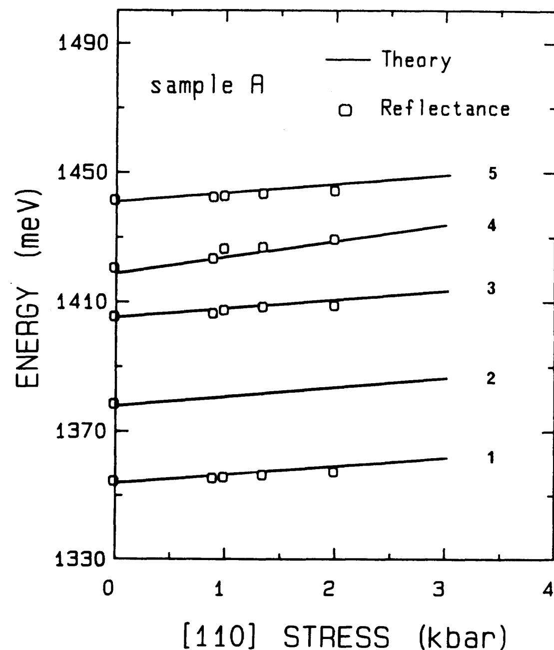

FIG. 7. Stress dependences of the reflectivity structures of sample A. The solid lines correspond to numerical calculations discussed in the text.

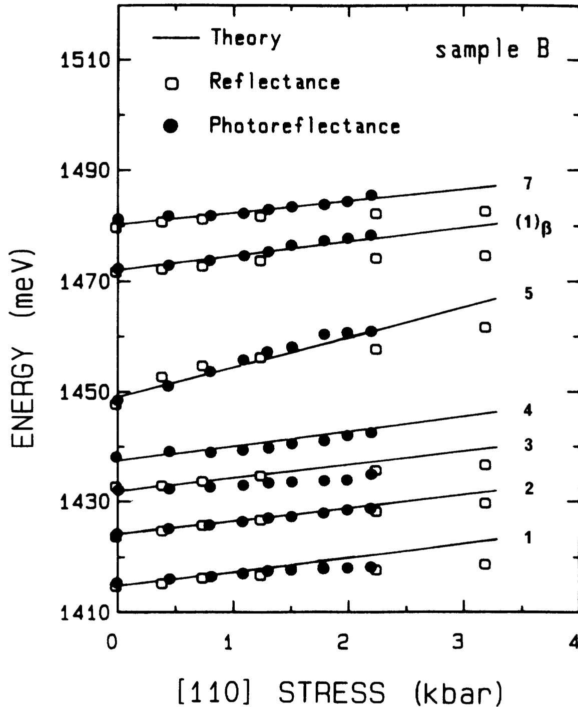

FIG. 8. Strain dependence of reflectivity and photoreflectivity structure of sample *B*. The transition label is the same as Fig. 3.

ing them a type-II system with respect to the electrons. This result is in agreement with other authors.[18] As a result of this configuration, both the light-hole exciton binding energy and its oscillator strength are small. This

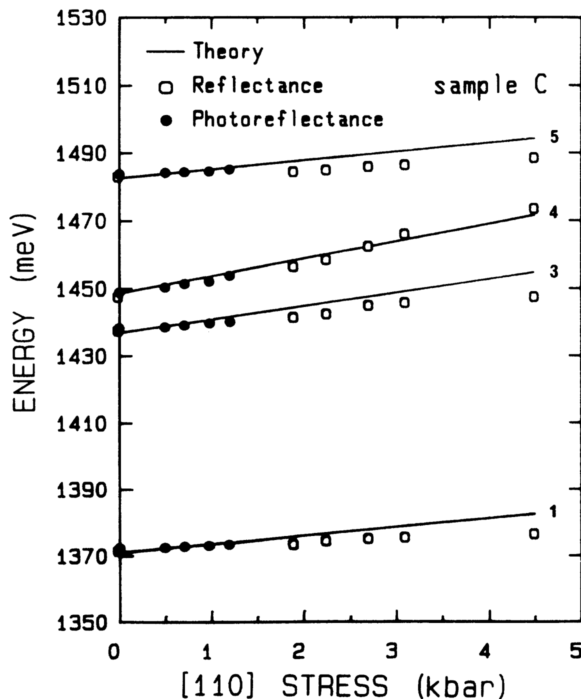

FIG. 9. Same as Fig. 8 for sample *C*.

agrees first with the fitting parameters given in Table III, where the light-hole exciton binding energies appear to be of the order of 4 meV, and secondly with the experimental spectra of Figs. 2–4 where the features associated with light-hole transitions are very weak.

Let us consider now the valence-band offset. We are able to adequately assign and understand all the experimental features, including those associated with the light-hole transitions, by using the mean value of 0.34 for the offset ratio Q_{vh}. This parameter has been extensively studied, since it is an essential parameter in accurately modeling the electronic and optical properties of quantum wells and superlattices. Our result is in reasonable agreement with reported values.[1–11] The discrepancy is thought to originate from the different lineup of the band structure for samples prepared under different conditions due to indium segregation.[45]

The band alignment in strained quantum wells results from the combined effects of a strain-free band offset for a hypothetical strain-free structure and the strain-induced shift of the conduction band and shift and splitting of the valence band. The strain-free valence-band offset, which is called the chemical band offset, is defined as $Q_V=\Delta E_v/\Delta E_g$, where ΔE_g and ΔE_v are, respectively, the band-gap and valence-band discontinuities between the strain-free isolated materials making up the QW. X-ray photoemission spectroscopy (XPS) has been used to study the chemical band offset in heterojunctions so as to obtain absolute values of ΔE_v,[53] independent of strain. In our samples, using Eqs. (4a) and (4b) together with Q_{vh} allows us to find Q_v. The estimated value is $Q_v \sim 12\%$, which is in good agreement with results obtained for the InAs-GaAs system from XPS measurements by using the Ga3*d* and In4*d* core levels, 15% (Ref. 21) and 20±8%.[53]

Following the feature assignments given in Table III and repeated in Figs. 2–4, let us briefly discuss the reflectance spectra. Figure 2 corresponding to the 110-Å SQW shows that the stronger features correspond to type-I, parity-allowed $e1$-$h1$ and $e2$-$h2$ transitions; the $e1$-l feature from the electron-light-hole type-II transitions is very weak and broad, as expected. However, in addition to these $\Delta n=0$ transitions, weak features associated with $e1$-$h2$ and $e1$-$h3$ transitions are seen. The $e1$-$h3$ transitions can be made allowed by band mixings[54] and by the finite barrier height, which induces different vanishing rates for electron and hole envelope functions into the wider-gap material, so that the resulting envelope-function overlap integral is not zero.[55] The observation of parity forbidden transitions, such as $e1$-$h2$, can be explained by band mixings[54] or by random alloy fluctuations which could destroy the symmetry of the system, as invoked in previous studies of $In_xGa_{1-x}As$-GaAs quantum wells.[56] Figure 3, which corresponds to sample *B*, characterized by low indium content, exhibits features associated to both the 270-Å $(QW)_\alpha$ and the 50-Å $(QW)_\beta$. The 50-Å QW has high confinement energies (63 meV for the electron and 29 meV for the heavy hole) due to its narrow well width ($L_W=52$ Å) and so gives rise to only one electron and one heavy-hole bound state. As a result, the reflectivity spectrum gives rise to only one feature, which is very strong and of course corresponds to the

$e1$-$h1$ exciton transition. The 270-Å well, in contrast, is wide enough to have three electron and five heavy-hole bound states, in spite of shallow potential wells (72 and 33 meV for the electron and heavy-hole wells, respectively). Parity-allowed and parity-forbidden transitions appear, but all the higher transitions are weak. Note that the $e3$-$h3$ parity-allowed transition is masked by the strong $e1$-$h1$ feature of the 50-Å QW. The 10-Å well in this sample can be observed in PL, but not by reflectivity. Its $e1$-$h1$ transition occurs at 1.482 eV, which is lost in the strong GaAs band-edge reflectance signal.

Figure 4 corresponds to sample C, which is a MQW composed by three QW's with nominal well width $L_w=70$ Å and barrier thickness $L_b=100$ Å. The calculated transition energies reported in Table III are obtained using the theoretical model given above, where the quantum wells are assumed to be uncoupled. This model calculation gives rise to an electron well depth of 120 meV with only one bound state and a heavy-hole well depth of 74 meV with two bound states. Figure 4 clearly shows a very strong feature associated with the $e1$-$h1$ ground-state transition and two other important features labeled $e1$-$h'3$ and $e'2$-$h2$. The first one corresponds to transitions between the electron bound state $e1$ and a resonant heavy-hole state labeled $h'3$. The second one corresponds to transitions between the heavy-hole bound state $h2$ and a resonant electron state $e'2$. Now, on account of the narrow barriers, $L_b=100$ Å, the three quantum wells are not strictly uncoupled. If we compare this system to the more commonly studied GaAs-AlAs, we note that the confining potentials are over an order of magnitude smaller (in GaAs-AlAs they are ~ 1000 meV for the electrons and ~ 500 meV for the holes[25]). The result is that, in $In_xGa_{1-x}As$-GaAs, coupling between confined states occurs for relatively thick layers of well and barrier.

We have used the transfer-matrix method in order to estimate the effects of the interwell coupling in our triple-quantum-well system. For states at $\mathbf{k}_\perp=0$, and without uniaxial stress, taking account of the continuity conditions at each of the six interfaces, we obtain an equation rather similar to the "classical" one given by Bastard[31] in the case of single quantum wells:

$$\prod_{i=1}^{3}(2\cos kL_i+\xi^-\sin kL_i)=A+B \ , \quad (11)$$

with

$$A=\xi^-(\xi^+)^2\left[\prod_{i=1}^{3}\sin kL_i\right] \times(e^{-2\rho h_1}+e^{-2\rho h_2}+e^{-2\rho(h_1+h_2)}) \ , \quad (12a)$$

$$B=2(\xi^+)^2(\sin kL_1\sin kL_2\cos kL_3 e^{-2\rho h_1} +\cos kL_1\sin kL_2\sin kL_3 e^{-2\rho h_2} +\sin kL_1\cos kL_2\sin kL_3 e^{-2\rho(h_1+h_2)}) \ . \quad (12b)$$

L_1, L_2, and L_3 are the widths of the well layers, while h_1 and h_2 are the widths of the intermediate barrier layers. The wave vectors k and ρ are given by $k^2=2m_w^*E/\hbar^2$, $\rho^2=2m_b^*(V-E)/\hbar^2$, where E is the energy, V is the potential well depth, and m_w^* and m_b^* are the effective masses of the carriers in the wells and in the barriers, respectively. We write $\xi=(\rho/k)(m_w^*/m_b^*)$, and introduce the quantities $\xi^{\pm}=\xi\pm 1/\xi$. In case of three identical quantum wells, the result is a lifting of the degeneracy of the single-well levels into three levels. In our samples $Lw_1=Lw_2=Lw_3=68$ Å and $Lb_1=Lb_2=100$ Å, and the corresponding confinement energies become (in meV) $e1^1=42.6$, $e1^2=43.6$, $e1^3=44.6$, $h1^1=12.60$, $h1^2=12.60$, $h1^3=12.60$, $h2^1=47.4$, $h2^2=47.5$, $h2^3=47.6$. Clearly, the hole states remain nearly degenerate, while the electron states become weakly split ($\sim\pm 1$ meV). This splitting of the electron ground state remains within the half width of the experimental reflectivity spectrum and cannot be observed. However, the photoreflectance spectrum (Fig. 5) clearly exhibits a fine structure in the $e1$-$h1$ feature, which may be related to this splitting of the electron state.

For the light holes, there are (see Fig. 10) two GaAs quantum wells with $L_w=100$ Å between three $In_xGa_{1-x}As$ barriers with $L_b=70$ Å. This configuration gives rise to metastable bound states. On account of the value of L_b, the lifetime of the light-hole inside the well should be longer than the exciton lifetime, so that the corresponding exciton transition may be observed. Unfortunately, the well depth is only 8.0 meV (see Table II) and the calculated confinement energy is only 5 meV, so that the transition energy associated with this metastable exciton should appear 6 meV above the $e1$-l type-II exciton. The spectrum given in Fig. 4 exhibits a shoulder located 6 meV above the feature $e1$-l, labeled y, which might be associated with this metastable exciton. The discrepancy between the experiment (~ 6 meV) and the calculation (~ 5 meV) may be the result of different values of the Rydberg energy of the two types of exciton.

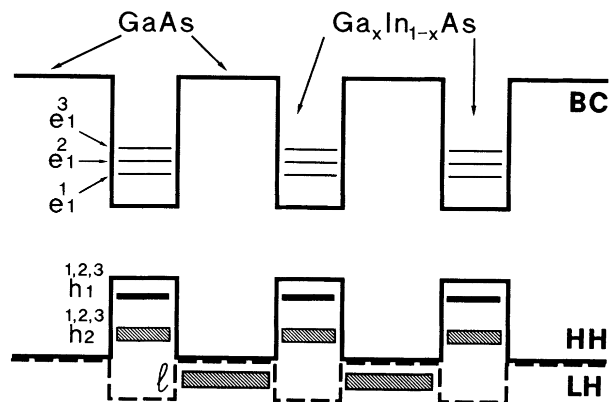

FIG. 10. Schematic energy-band diagram for the MQW of sample C, which shows three quantum wells for the electron and heavy hole and two quantum wells for the light-hole. In the $In_xGa_{1-x}As$ layers the top of the valence band is split into heavy-hole (HH) and light-hole (LH) bands as a result of the lattice-mismatch strain.

Although the shoulder labeled y in Fig. 4 is very weak, its stress dependence has been observed: it appears to parallel the $e1$-l feature, which confirms the electron-light-hole assignment.

IV. CONCLUSION

The uniaxial stress dependences of reflectance and photoreflectance spectra have been studied for single and multiple $In_xGa_{1-x}As$-GaAs strained quantum wells grown with several well widths and two indium contents. The stress dependence of the spectra permits an unambiguous assignment of the experimental features to electron-heavy-hole and electron-light-hole exciton transitions. Comparison of the experimental intersubband energies with an envelope-function calculation, taking into account the misfit-strain-induced coupling between the light-hole valence band and the split-off band, yields values of the of the physical parameters, indium contents, and well widths in good agreement with those deduced from the growth conditions. We find a valence-band offset ratio $Q_{vh}=\Delta E_{vh}/\Delta E_{gh}$ of about 34%, in reasonable agreement with earlier results. This value implies that the light-hole states are type II, in agreement with Refs. 1, 2, and 7–11.

[1]D. J. Arent, K. Deneffe, C. Van Hoof, J. De Brook, and G. Borgh, in *Band Structure Engineering of Semiconductor Microstructures,* edited by R. A. Abram and M. Jaros, NATO ARW Series Vol. 189 (Plenum, New York, 1988), p. 303.

[2]N. G. Anderson, Y. C. Lu, and R. M. Kolbas, in *Interfaces, Superlattices, and Thin Films,* edited by J. D. Dow and I. K. Schuller, MRS Symposia Proceedings No. 77 (Materials Research Society, Pittsburgh, 1987), p. 437.

[3]E. S. Koteles, B. Elman, P. Melman, D. C. Bertolet, J. K. Hsu, and K. M. Lau, in *Proceedings of the 20th International Conference on the Physics of Semiconductors, Thessaloniki, 1990,* edited by E. M. Anastassakis and J. D. Joannopoulos (World Scientific, Singapore, 1990), Vol. 2, p. 965.

[4]D. C. Reynolds, K. R. Evans, K. K. Bajaj, B. Jogai, C. E. Stutz, and P. W. Yu, Phys. Rev. B **43**, 1871 (1991).

[5]J. Menendez, A. Pinczuk, D. J. Werder, S. K. Sputz, R. C. Miller, D. L. Sivco, and A. Y. Cho, Phys. Rev. B **36**, 8165 (1987).

[6]J. Y. Marzin, M. N. Charasse, and B. Sermage, Phys. Rev. B **31**, 8298 (1985).

[7]P. Voisin, M. Voos, J. Y. Marzin, M. C. Tamargo, R. E. Nahory, and A. Y. Cho, Appl. Phys. Lett. **48**, 1476 (1986).

[8]I. J. Fritz, B. L. Doyle, T. J. Drummond, R. M. Biefield, and G. C. Osborn, Appl. Phys. Lett. **48**, 1606 (1986).

[9]T. G. Anderson, Z. G. Chen, V. D. Kulokovskii, A. Uddin, and J. T. Vallin, Appl. Phys. Lett. **51**, 752 (1987).

[10]G. Ji, D. Hwang, W. K. Reddy, T. S. Henderson, R. Houdre, and H. Morkoç, J. Appl. Phys. **62**, 3366 (1987).

[11]S. H. Pan, H. Shen, Z. Hang, F. H. Pollak, W. Zhuang, Q. Xu, A. P. Roth, R. A. Masut, C. Laselle, and D. Morris, Phys. Rev. B **38**, 3375 (1988).

[12]B. Y. Hua, E. Fortin, A. P. Roth, and R. A. Masut, Appl. Phys. Lett. **53**, 1062 (1988).

[13]S. Niki, C. L. Lin, W. S. C. Chang, and H. H. Wieder, Appl. Phys. Lett. **55**, 1339 (1989).

[14]J. D. Lambkin, L. K. Howard, and M. T. Emeny, Phys. Rev. B **42**, 1738 (1990).

[15]H. Q. Hou, L. J. Wang, R. M. Tang, and J. M. Zhou, Phys. Rev. B **42**, 2926 (1990).

[16]H. Q. Hou, Y. Segawa, Y. Aoyagi, S. Namba, and J. M. Zhou, Phys. Rev. B **42**, 1284 (1990).

[17]N. J. Pulsford, R. J. Nicholas, R. J. Warburton, G. Duggan, K. J. Moore, K. Woodbridge, and C. Roberts, Phys. Rev. B **43**, 2246 (1991).

[18]J. M. Gerard and J. Y. Marzin, Phys. Rev. B **40**, 6450 (1989).

[19]S. P. Kowalczyk, W. J. Schaffer, E. A. Kraut, and R. W. Grant, J. Vac. Sci. Technol. B **20**, 705 (1982).

[20]A. G. Milnes and D. L. Feucht, *Heterojunctions and Metal Semiconductors Junctions* (Academic, New York, 1972), p. 8.

[21]W. A. Harrison and J. Tersoff, J. Vac. Sci. Technol. B **4**, 1068 (1986).

[22]C. G. Van de Walle and R. Martin, Phys. Rev. B **35**, 8154 (1987).

[23]V. A. Wilkinson, A. D. Prins, D. J. Dunstan, L. K. Howard, and M. T. Emeny, J. Electron. Mater. **20**, 509 (1991).

[24]B. Gil, P. Lefebvre, H. Mathieu, G. Platero, M. Altarelli, T. Fukunaga, and H. Nakashima, Phys. Rev. B **38**, 1215 (1988).

[25]P. Lefebvre, B. Gil, H. Mathieu, and R. Planel, Phys. Rev. B **39**, 5550 (1989); **40**, 7802 (1989).

[26]P. Lefebvre, P. Bonnel, B. Gil, and H. Mathieu, Phys. Rev. B **44**, 5635 (1991), and references cited therein.

[27]B. Gil, P. Lefebvre, P. Boring, K. J. Moore, G. Duggan, and K. Woodbridge, Phys. Rev. B **44**, 1942 (1991).

[28]H. Mathieu, P. Merle, E. L. Ameziane, B. Archilla, J. Camassel, and G. Poiblaud, Phys. Rev. B **19**, 2209 (1979).

[29]Y. L. Leu, F. A. Thiel, H. Scheider, B. I. Miller, and J. Backmann, J. Electron. Mater. **8**, 663 (1979).

[30]O. Berolo and J. C. Wooley, in *Proceedings of the 11th International Conference on the Physics of Semiconductors, Warsaw, 1972,* edited by M. Miasek and J. Rauluszkiewicz (Polish Scientific, Warsaw, 1972), p. 1420.

[31]G. Bastard, in *Wave Mechanics Applied to Semiconductor Heterostructures* (Les Editions de Physique, Paris, 1988), pp. 246–250.

[32]*Semiconductors Group IV Element and III-V Compounds Data in Science and Technology,* edited by O. Madelung (Springer-Verlag, Berlin, 1991).

[33]D. Gerlich, J. Appl. Phys. **34**, 2915 (1963).

[34]V. A. Wilkinson, A. D. Prins, J. D. Lambkin, E. P. O'Reilly, D. J. Dunstan, L. K. Howard, and M. T. Emeny, Phys. Rev. B **42**, 3113 (1990).

[35]E. P. O'Reilly, Semicond. Sci. Technol. **4**, 121 (1989).

[36]D. D. Nolte, W. Walvkiewicz, and E. E. Haller, Phys. Rev. Lett. **59**, 501 (1987).

[37]A. Gavini and M. Cardona, Phys. Rev. B **1**, 672 (1970).

[38]H. Chandrasekhar and F. H. Pollak, Phys. Rev. B **15**, 2127 (1977).

[39]P. Y. Yu, M. Cardona, and F. H. Pollak, Phys. Rev. B **3**, 340 (1971).

[40]P. Lawaetz, Phys. Rev. B **4**, 3460 (1971).

[41]K. J. Moore, G. Duggan, K. Woodbridge, and C. Roberts, Phys. Rev. B **41**, 1090 (1990).

[42]M. J. L. S. Haines, N. Ahmed, S. J. A. Adams, K. Mitchell, I. R. Agool, C. R. Pidgeon, B. C. Cavenett, E. E. O'Reilly, A. Ghiti, and M. T. Emeny, Phys. Rev. B **43**, 11 944 (1991).

[43]M. T. Emeny, L. K. Howard, K. P. Homewood, J. D. Lamb-

kin, and C. R. Whitehouse, J. Cryst. Growth **111**, 413 (1991).

[44]J. D. Lambkin, L. K. Howard, and M. T. Emeny, Phys. Rev. B **42**, 1738 (1990).

[45]K. Woodbridge, K. J. Moore, N. L. Andrew, and P. F. Fewster, J. Cryst. Growth **11**, 339 (1991).

[46]R. H. Dixon and P. J. Goodhew, J. Appl. Phys. **68**, 3163 (1990).

[47]D. J. Dunstan, P. Kidd, L. K. Howard, and R. H. Dixon, Appl. Phys. Lett. **59**, 3390 (1991).

[48]Y. Chen, B. Gil, and H. Mathieu, Ann. Phys. (Paris) **12**, 109 (1987), and references cited therein.

[49]H. Mathieu, J. Allègre, and B. Gil, Phys. Rev. B **43**, 2218 (1991), and references cited therein.

[50]D. A. Aspnes, in *Handbook of Semicondutors,* edited by T. S. Moss (North-Holland, Amsterdam, 1980), Vol. 2, p. 109.

[51]B. V. Shanabrook, D. J. Glemboki, and W. T. Beard, Phys. Rev. B **35**, 2540 (1987).

[52]H. Shen, P. Parayanthal, F. H. Pollak, M. Tombiewiez, T. J. Drummond, and J. N. Schulman, Appl. Phys. Lett. **48**, 653 (1986).

[53]R. W. Grant, E. A. Krant, J. R. Waldrop, and S. P. Kowalczyk, in *Heterojunction Band Discontinuities,* edited by F. Capasso, and G. Margaritondo (North-Holland, Amsterdam, 1987), Chap. 4, p. 167.

[54]R. C. Miller, A. C. Gossard, G. D. Sanders, Y. C. Chang, and J. N. Schulman, Phys. Rev. B **32**, 8452 (1985), and references cited therein.

[55]Z. M. Fang, A. Persson, and R. M. Cohen, Phys. Rev. B **37**, 4071 (1988).

[56]R. L. S. Devine, and W. T. Moore, Solid State Commun. **65**, 177 (1988).